A Cross-Linkable Donor Polymer as the Underlying Layer to Tune the Active Layer Morphology of Polymer Solar Cells

Bin Meng, Zaiyu Wang, Wei Ma, Zhiyuan Xie, Jun Liu,* and Lixiang Wang*

For polymer solar cells (PSCs) with conventional configuration, the vertical composition profile of donor:acceptor in active layer is detrimental for charge carrier transporting/collection and leads to decreased device performance. A cross-linkable donor polymer as the underlying morphology-inducing layer (MIL) to tune the vertical composition distribution of donor:acceptor in the active layer for improved PSC device performance is reported. With poly(thieno[3,4-*b*]-thiophene/benzodithiophene):[6,6]-phenyl C_{71}-butyric acid methyl ester (PTB7:$PC_{71}BM$) as the active layer, the MIL material, PTB7-TV, is developed by attaching cross-linkable vinyl groups to the side chain of PTB7. PSC device with PTB7-TV layer exhibits a power conversion efficiency (PCE) of 8.55% and short-circuit current density (J_{SC}) of 15.75 mA cm^{-2}, in comparison to PCE of 7.41% and J_{SC} of 13.73 mA cm^{-2} of the controlled device. The enhanced device performance is ascribed to the much improved vertical composition profile and reduced phase separation domain size in the active layer. These results demonstrate that cross-linked MIL is an effective strategy to improve photovoltaic performance of conventional PSC devices.

1. Introduction

Morphology of donor:acceptor blend in active layer of polymer solar cells (PSCs) plays an important role in charge separation, transport, and collection, thus is a major factor to determine the PSC device performance.[1] It is widely accepted that the ideal morphology should be a bicontinuous interpenetrating network with a phase domain size of 10–20 nm.[2] Moreover, to facilitate charge transport and charge collection by the electrodes, the ideal morphology should have a vertical composition profile with the donor accumulating at the anode side and the acceptor enriched at the cathode side.[3] For spin-coating of active layer in conventional device structure, owing to the much larger surface energy of anode interlayer (normally poly(3,4-ethylenedioxy-thiophene) doped with poly(styrenesulfonate) (PEDOT:PSS), γ = 91.6 mJ m^{-2}) than the air (γ = 0), the donor with small surface energy (γ = 20–22 mJ m^{-2}) would prefer to enrich at the top (cathode side) and the acceptor with larger surface energy (γ = 29 mJ m^{-2}) would prefer to enrich at the bottom (anode side).[4] This vertical distribution of donor:acceptor is detrimental for charge carrier transporting/collection and leads to decreased PSC device performance. One effective approach to improve the vertical distribution of active layer is to use solvent additive, in which the solvent additive with high boiling point can dramatically change the film-forming kinetics and consequently change the blend morphology. For example, Wu et al.[5] and Park and co-workers[6] have used specific solvent additives, which can selectively interact with the donor or the acceptor, to alter the vertical distribution in the active layer. Huang and co-workers[7] have obtained the desired compositionally graded active layer using methanol treatment to extract the acceptor to the top surface of active layer. However, the solvent additive approach is only applicable for a portion of PSCs because many high efficiency PSCs use single solvent without solvent additive.[8] Therefore, it remains a great challenge to develop an alternative strategy to control the vertical phase separation of PSCs.

The active layer morphology of PSCs is affected by the surface property of the underlying layer.[9] We have demonstrated an approach to improve the active layer morphology by using a phosphonate polymer spin-coated on PEDOT:PSS surface as the morphology-inducing layer (MIL).[10] However, the fabrication of multilayer PSC devices requires orthogonal solvent processing, which constrains the choice of processing solvent and leads to limited device performance.

Here, we use a cross-linkable polymer as the underlying MIL to tune the vertical composition distribution of donor:acceptor blend in the active layer, which provides solvent selection flexibility to process active layer and leads to improved PSC device performance. As shown in **Scheme 1**, with poly(thieno[3,4-*b*]-thiophene/benzodithiophene):[6,6]-phenyl C_{71}-butyric acid methyl ester (PTB7:$PC_{71}BM$) as the active layer,[11] we develop the MIL material, poly{[4,8-bis[(undec-10-enyl)oxy]benzo[1,2-*b*:4,5-*b*′]dithiophene-2,6-diyl][3-fluoro-2-[(2-ethylhexyl)carbonyl]-thieno-[3,4-*b*]-thiophenediyl]} (**PTB7-TV**), in which cross-linkable vinyl groups

B. Meng, Dr. Z. Y. Xie, Prof. J. Liu, Prof. L. X. Wang
State Key Laboratory of Polymer Physics and Chemistry
Changchun Institute of Applied Chemistry
Chinese Academy of Sciences
Changchun 130022, P. R. China
E-mail: liujun@ciac.ac.cn

B. Meng
University of Chinese Academy of Sciences
Beijing 100039, P. R. China

Z. Y. Wang, Prof. W. Ma
State Key Laboratory for Mechanical Behavior of Materials
Xi'an Jiaotong University
Xi'an 710049, P. R. China
E-mail: msewma@mail.xjtu.edu.cn

DOI: 10.1002/adfm.201503833

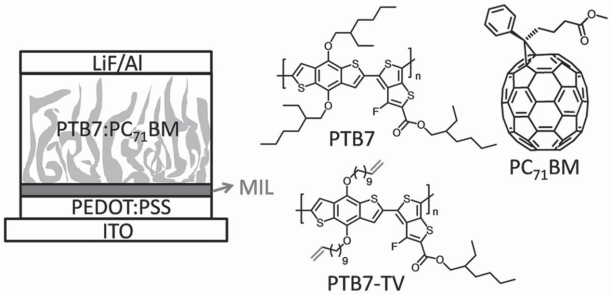

Scheme 1. PSC device structure, chemical structures of the donor and acceptor in the active layer, chemical structure of **PTB7-TV**.

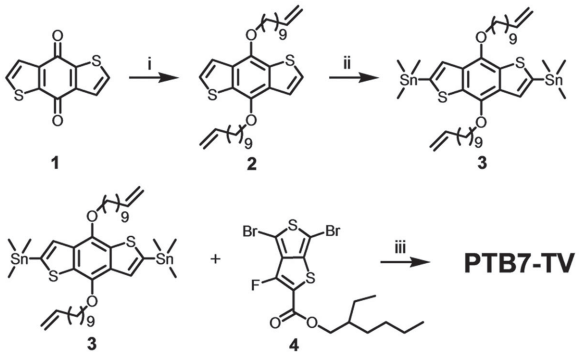

Scheme 2. Synthetic route of **PTB7-TV**. Reagents and conditions: i) Zn, NaOH, H_2O, 105 °C, 1.5 h; then 11-bromo-1-undecane, tetrabutylammonium bromide, 15 h. ii) *n*-BuLi, THF, −78 °C, 2 h; then Me_3SnCl, −78 °C to room temperature, overnight. iii) $Pd_2(dba)_3$, P(*o*-tolyl)$_3$, toluene/DMF, 120 °C, 36 h.

are attached to the side chain of PTB7. While the controlled device without MIL shows the power conversion efficiency (PCE) of 7.41%, the PSC device with **PTB7-TV** as MIL exhibits the PCE of 8.55% owing to the much improved vertical composition profile, reduced phase separation domain size, and reserved average domain purity in the active layer. These results demonstrate that cross-linked MIL is an effective strategy to improve photovoltaic performance of conventional PSC devices.

2. Results and Discussion

As shown in Scheme 1, **PTB7-TV** has the identical conjugated backbone with that of PTB7 and contains terminal vinyl group at the side chain. Therefore, **PTB7-TV** is expected to have similar lowest unoccupied molecular orbital (LUMO)/highest occupied molecular orbital (HOMO) energy levels with those of PTB7, which would not introduce additional energy barrier for charge transport when used as MIL.[12] The terminal vinyl groups at the side chain of **PTB7-TV** can cross-link to give a robust film,[13] which would be resistant against solvent and enable spin-coating of active layer on top of it. Moreover, the low-polarity intrinsic of **PTB7-TV** is expected to give a small surface energy of the MIL and should be beneficial for the improved vertical composition distribution in the active layer.[9]

The synthetic route of **PTB7-TV** is outlined in **Scheme 2**. Starting from benzo[1,2-*b*:4,5-*b*′]dithiophene-4,8-dione (**1**), we obtained 4,8-bis(undec-10-enyloxy)benzo[1,2-*b*:4,5-*b*′]dithiophene (**2**) with an overall high yield of 67% after reduction, deprotonation, and subsequent alkylation. The key monomer **3** was synthesized from **2** through stannylation reaction. Finally, the di-tin monomer **3** was copolymerized with the di-bromo monomer **4** using Stille polymerization to afford the target polymer **PTB7-TV** with a high yield of 80%. Gel permeation chromatography (GPC) with monodisperse polystyrene (PS) as the standards indicates its number-average molecular weight (M_n) of 15 200 with polydispersity index (PDI) of 3.5. According to the study by Yu and co-workers,[14] the low M_n and large PDI suggest that PTB7-TV should show moderate PSC device performance when used as the polymer donor in the active layer. According to thermogravimetric analysis, **PTB7-TV** is stable up to 330 °C.

Cyclic voltammetry is employed to estimate the HOMO/LUMO energy levels of **PTB7-TV** and PTB7. As shown in **Figure 1**a, the two polymers exhibit oxidation/reduction waves with similar onset oxidation/reduction potentials due to their identical conjugated backbones. According to the formula, ($E_{HOMO} = -(4.8 + E_{onset}^{ox})$ eV, $E_{LUMO} = -(4.8 + E_{onset}^{red})$ eV), the HOMO/LUMO energy levels of **PTB7-TV** and PTB7 are estimated to be −5.15 eV/−3.24 eV and −5.23 eV/−3.31 eV, respectively (see **Table 1**). As shown in Figure 1b,

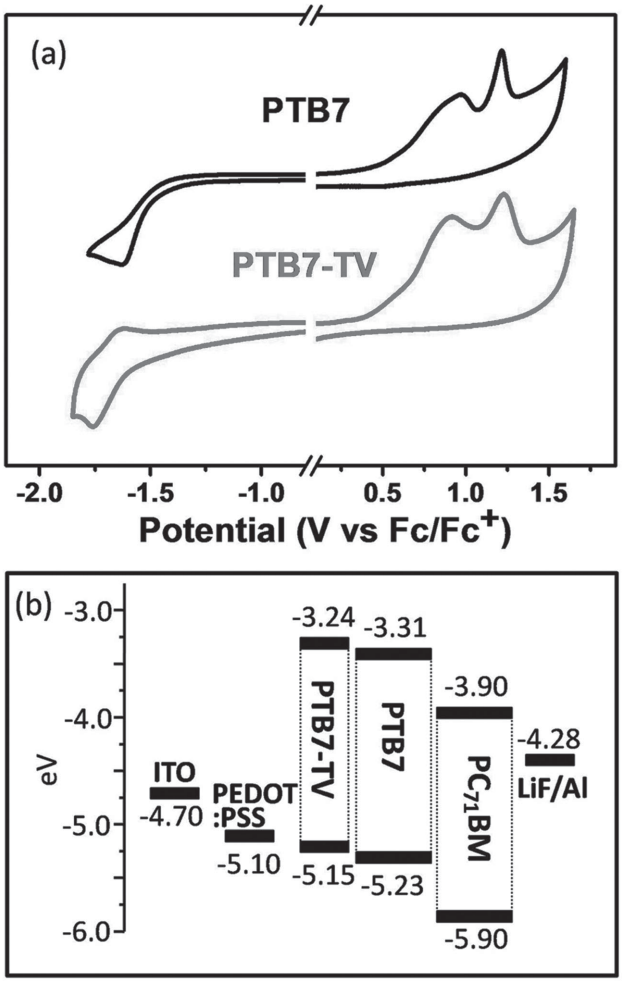

Figure 1. a) Cyclic voltammogram of PTB7 and **PTB7-TV**. b) Energy level diagrams of PSCs with **PTB7-TV** as MIL.

DOI: 10.1002/adfm.201503833

Table 1. Photophysical and electrochemical properties of **PTB7-TV** and PTB7.

Polymer	E_{onset}^{ox} a) [V]	E_{onset}^{red} a) [V]	HOMO [eV]	LUMO [eV]	E_g^{ec} [eV]	λ_{max}^{sol} [nm]	λ_{max}^{film} [nm]	λ_{onset}^{film} [nm]	E_g^{opt} [eV]
PTB7-TV	0.35	−1.56	−5.15	−3.24	1.91	641	658	757	1.64
PTB7	0.43	−1.49	−5.23	−3.31	1.92	676	677	738	1.68

a)Onset potential versus Fc/Fc^+.

with the similar HOMO/LUMO energy levels of the two polymers, the introduction of **PTB7-TV** layer in the PSC device of PTB7:$PC_{71}BM$ would not cause energy barrier for hole transport.

The absorption spectra of **PTB7-TV** and PTB7 in chlorobenzene (CB) solution and in thin film are shown in Figure S1 in the Supporting Information. Compared with that of PTB7, the absorption spectrum of **PTB7-TV** is broader with blueshifted absorption maxima and redshifted onset absorption wavelength. According to the study by Yu and co-workers,[14] the broad absorption spectrum of **PTB7-TV** is related to the large PDI, which is usually ascribing to the structure defects in polymer chain.

To enable the fabrication of multilayer PSC device with MIL, a key requirement for MIL material is that the MIL should not be dissolved by the solvent used for spin-coating of the active layer. With the terminal vinyl groups, **PTB7-TV** is able to cross-link under UV irradiation and heating at 130 °C. The cross-linking is indicated by the disappearance of the peak at 1640 cm^{-1} in the fourier transform infrared (FTIR) spectra, which is assigned to the terminal vinyl group of pristine **PTB7-TV** (Figure S2, Supporting Information).[15] Furthermore, we wash the cross-linked film of **PTB7-TV** with CB (the solvent to process the active layer of PSCs) to test its resistance to the organic solvent. **Figure 2** shows the absorption spectra of the film before and after the solvent washing. The absorbance of the cross-linked **PTB7-TV** film keeps almost unchanged after washing with CB, suggesting that cross-linked **PTB7-TV** is robust enough to be used as MIL in multilayer PSC devices.

Since the surface energy of the underlying layer plays an important role in the film formation process and affects the active layer morphology of PSCs, we estimate the surface energy of **PTB7-TV** and the state-of-the-art anode interlayer PEDOT:PSS. **Figure 3**a–d shows the image of droplets of water and ethylene glycol on the surface of cross-linked **PTB7-TV** and PEDOT:PSS. According to the water contact angles, **PTB7-TV** surface is hydrophobic while PEDOT:PSS surface is hydrophilic. The surface energies are estimated based on the contact angles with water and ethylene glycol droplets and according to the Owens and Wendt equation.[16] In comparison to PEDOT:PSS with a large surface energy of 91.6 mJ m^{-2}, cross-linked **PTB7-TV** film has a much smaller surface energy of 20.5 mJ m^{-2}. Since the large surface energy of PEDOT:PSS results in the undesired vertical composition distribution of active layer in PSCs, the small surface energy of **PTB7-TV** would be beneficial for improved active layer morphology of PSCs.

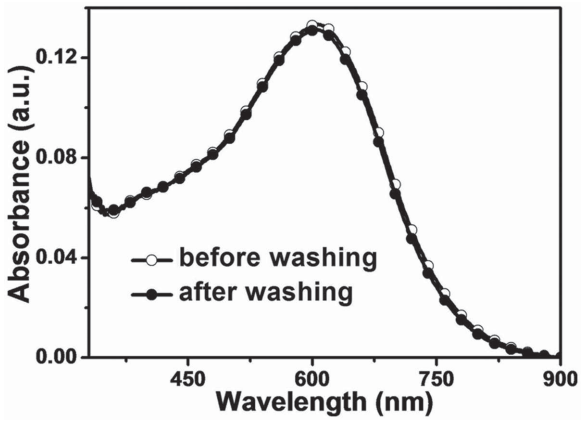

Figure 2. Absorption spectra of cross-linked **PTB7-TV** film before and after washing with CB.

To investigate the application of **PTB7-TV** as MIL, we fabricated PSC devices with the configuration of indium tin oxide/PEDOT:PSS (30 nm)/**PTB7-TV** (2 nm)/PTB7:$PC_{71}BM$ (100 nm)/LiF (1 nm)/Al (100 nm). **PTB7-TV** was spin-coated with its CB solution, followed by cross-linking under UV irradiation (λ = 254 nm, 12 W) at 130 °C for 30 min. Then, the PTB7:$PC_{71}BM$ active layer was deposited on **PTB7-TV** layer by spin-coating with the CB solution containing 3% 1,8-diiodooctane. For comparison, a controlled device without **PTB7-TV** layer was also fabricated. **Figure 4**a shows the current density–voltage (J–V) characteristic of the devices. The controlled device exhibits PCE of 7.41% with open-circuit voltage (V_{OC}) of 0.75 V, short-circuit current (J_{SC}) of 13.73 mA cm^{-2}, and fill factor (FF) of 0.72 (see **Table 2**). In comparison, the device with **PTB7-TV** as MIL shows V_{OC} of 0.75 V, J_{SC} of 15.75 mA cm^{-2}, and FF of 0.72, corresponding to PCE of 8.55%. The two devices have virtually identical parameters, except for a 15% increase in J_{SC} for the device with **PTB7-TV** as MIL. The increase in J_{SC} is further confirmed by the higher external quantum efficiency (EQE) of the device with **PTB7-TV** than that of the controlled device (Figure 4b). Considering that the incorporation of thin **PTB7-TV** layer does not increase the absorption of the active layer (see Figure S6 in the Supporting Information), the obviously increased J_{SC} may be ascribed to the change of blend morphology. It is worthy to note that the device performance with **PTB7-TV** as MIL is among the best reported for PSCs based on PTB7 with conventional configuration.[17]

The increased J_{SC} and PCE with **PTB7-TV** layer is mainly due to the effect of the underlying **PTB7-TV** layer on the morphology of PTB7:$PC_{71}BM$ active layer. X-ray photoelectron spectroscopy (XPS) was used to estimate the composition of the PTB7:$PC_{71}BM$ active layer at different depth. The *F*1s peak comes from PTB7 and can be referred as the signature of PTB7. The *C*1s peak represents the sum of PTB7 and $PC_{71}BM$. Therefore, the *F*1s/*C*1s peak area ratio can be correlated to the content of PTB7 in the blend. **Figure 5** shows the dependence of the "F_{1s}/C_{1s} peak area ratio" as a function of the film depth of active layer (0, 20, 40, 70, and 100 nm). For

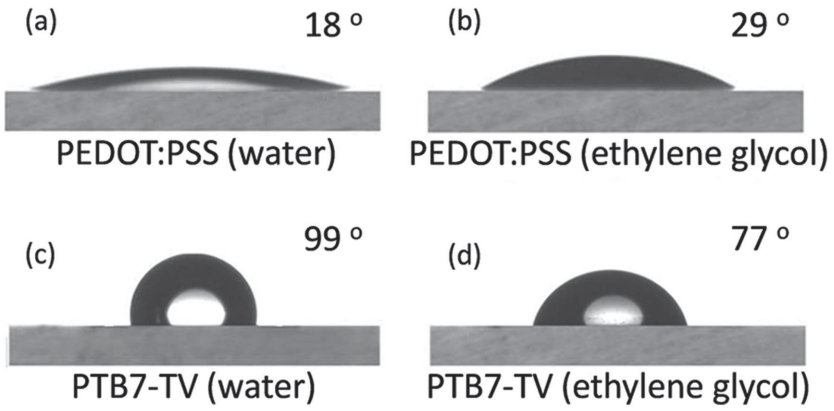

Figure 3. a,c) Droplets of water and b,d) ethylene glycol on the surface of a,b) PEDOT:PSS and c,d) cross-linked **PTB7-TV**. The contact angles are shown.

the top surface of the active layer (depth of 0 nm), the F_{1s}/C_{1s} ratio is lower for the device with **PTB7-TV** compared to the controlled device. This indicates that the application of **PTB7-TV** layer leads to less donor polymer accumulating on the top surface of the active layer, which is beneficial for the electron collection by the cathode in the PSC devices. The controlled device exhibits the decrease of F_{1s}/C_{1s} ratio with the increasing depth, suggesting that the content of the donor polymer gradually decreases toward the PEDOT:PSS surface. In contrast, the increased F_{1s}/C_{1s} ratio with increased depth for the device with **PTB7-TV** layer indicates that the donor polymer is gradually enriched toward the anode side. This vertical composition profile is beneficial for hole transporting to the anode and electron transporting to the cathode and may explain the increased J_{SC} and PCE of the device with **PTB7-TV**.[18] It is widely accepted that morphology of polymer blends is affected by the surface energy of the underlying layer. The much reduced surface energy with **PTB7-TV** spin-coated on PEDOT:PSS leads to the improved vertical compositional profile of PTB7:$PC_{71}BM$ blend in the active layer.

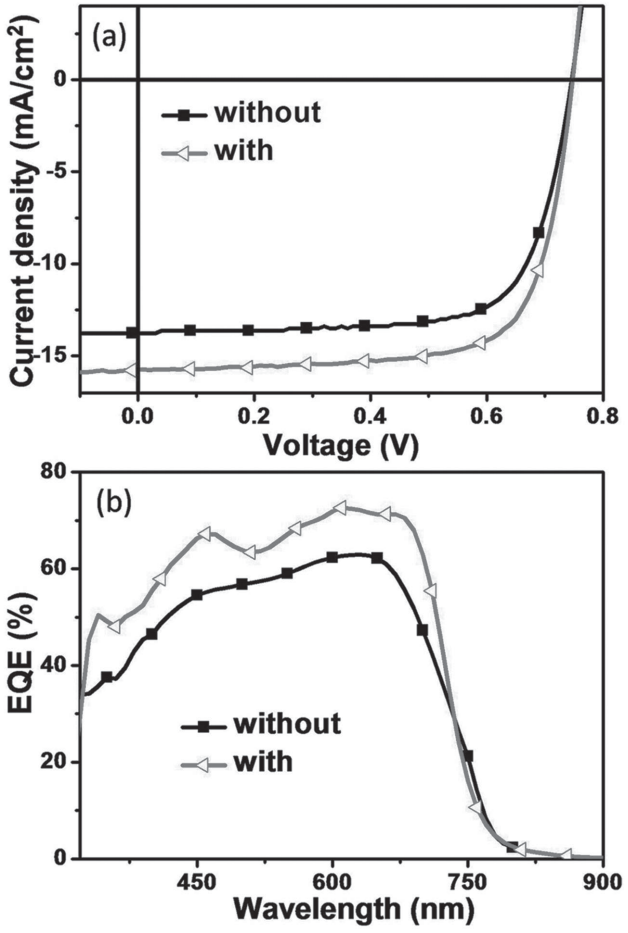

Figure 4. a) *J–V* curves and b) EQE curves of PSC devices with and without **PTB7-TV** as MIL.

For completely disclosing the change of blend morphology with and without **PTB7-TV** as MIL, the morphology of active layers was also investigated by grazing incident wide-angle X-ray scattering (GIWAXS)[19] and resonant soft X-ray scattering (R-SoXS).[20] First, we examined the difference of crystalline nature in the two blends with and without **PTB7-TV** as MIL using GIWAXS. **Figure 6** presents the GIWAXS 2D patterns and line-cut profiles in the in-plane (q_{xy} axis) and out-of-plane (q_z axis) direction. In 2D patterns, the weak peak at $q \approx 1.8$ Å^{-1} in out-of-plane direction is PTB7 π–π stacking peak. The absence of this peak in in-plane direction suggests that PTB7 has a preferential face-on orientation with regard to the substrate. Lamellar stacking (100) and (200) peaks at $q \approx 0.33$ and 0.66 Å^{-1} are observed in the in-plane direction. When comparing blend with and without underlying **PTB7-TV** layer, subtle differences between two blends indicate that the existence of **PTB7-TV** layer does not have great changes on the crystallinity of the blend.

To profoundly reveal the difference between the two blends fabricated with and without **PTB7-TV** as MIL, the distributions of domain spacing as well as relative domain purities were recorded through R-SoXS. A photon energy of 284.2 eV is selected to provide highly enhanced contrast between components. The results were shown in **Figure 7**. The blend without **PTB7-TV** exhibits a scattering peak at $q \approx 0.08$ nm^{-1}, which corresponds to about 80 nm characteristic phase separation length scale, whereas the blend with **PTB7-TV** shows a scattering peak at $q \approx 0.12$ nm^{-1}, which is equal to ≈ 50 nm characteristic phase separation length scale. The phase separation length scale is obtained through the caculated mode of $2\pi/q$. These results are consistent with the phase separation revealed by transmission electron microscopy

Table 2. Characteristics of the PSC devices with and without **PTB7-TV** as MIL.

Device	V_{OC} [V]	J_{SC} [mA cm^{-2}]	FF	PCE [%]
Without	0.75	13.73	0.72	7.41
With	0.75	15.75	0.72	8.55

Adv. Funct. Mater. **2015**,
DOI: 10.1002/adfm.201503833

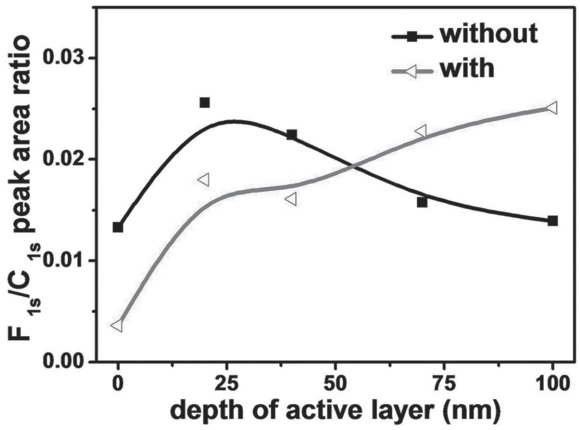

Figure 5. Dependence of the "F_{1s}/C_{1s} peak area ratio" in XPS spectra on the depth of the PTB7:$PC_{71}BM$ active layer.

(TEM) (as shown in Figure S4 in the Supporting Information). The difference on characteristic phase separation length scale indicates that the blend with **PTB7-TV** layer induces smaller phase separation than the blend without **PTB7-TV**. The smaller domain is beneficial for charge separation, and thus could increase J_{sc}. Relative domain purity of two blends are also compared by calculating the total scattering intensity, which is got by integrating the scattering profiles over the measurable q range.[20c,21] Purity values of the two blends are close, indicating that **PTB7-TV** has little influence on relative domain purity. It is reported that relative domain purity is crucial for bimolecular recombination and thus FF.[20c,22] The similar relative domain purity revealed here is consistent with the similar FF in the devices with and without **PTB7-TV** as MIL.

3. Conclusion

In summary, we have developed a cross-linkable donor polymer **PTB7-TV** as MIL to optimize the active layer morphology and enhance the photovoltaic performance of PTB7:$PC_{71}BM$-based PSC devices. With **PTB7-TV** spin-coated on PEDOT:PSS, the much smaller surface energy of the underlying layer leads to improved vertical composition profile and reduced phase separation domain size in the active layer. The resulting PSC device with **PTB7-TV** as MIL exhibits PCE of 8.55%, in comparison to PCE of 7.41% of the controlled device. These results demonstrate that cross-linked MIL is an effective approach to optimize active layer morphology and improve photovoltaic performance of conventional PSC devices.

4. Experimental Section

Synthesis of 4,8-Bis(Undec-10-Enyloxy) Benzo[1,2-b:4,5-b′]Dithiophene (**2**): To a 50 mL three-necked flask, benzo[1,2-b:4,5-b′]dithiophene-4,8-dione (0.40 g, 1.82 mmol), zinc powder (0.31 g, 4.72 mmol), sodium hydroxide (1.09 g, 27.30 mmol), and 10 mL degassed water were added successively under argon atmosphere. The reaction mixture was heated to reflux and stirred for 1.5 h. Then, 11-bromoundec-1-ene (0.96 mL, 4.37 mmol) and tetrabutylammonium bromide (35.2 mg, 0.11 mmol) were added under argon atmosphere. The resulting solution was continuously stirred at 100 °C for another 15 h. After workup, the reaction mixture was poured into deionized water and extracted with ethyl acetate for three times. The combined organic phase was washed with brine, dried over anhydrous Na_2SO_4, filtered, and concentrated. Finally, the residual was purified by silica gel column chromatography with petroleum ether/dichloromethane = 15/1 as eluent to afford the title compound as a yellow oil (0.67 g, 67%). ^{1}H NMR (400 MHz, $CDCl_3$), δ (ppm): 7.47 (*d*, *J* = 5.5 Hz, 1H), 7.36 (*d*, *J* = 5.5 Hz, 1H), 5.88–5.75 (m, 1H), 5.04–4.90 (m, 2H), 4.27 (*t*, *J* = 6.6 Hz, 2H), 2.08–2.00 (m, 2H), 1.90–1.80 (m, 2H), 1.61–1.51 (m, 2H), 1.44–1.25 (m, 10H). ^{13}C NMR (101 MHz, $CDCl_3$) δ (ppm): 144.55, 139.24, 131.61, 130.16, 125.97, 120.32, 114.13, 73.94, 33.82, 30.54, 29.55, 29.43, 29.13, 28.94, 26.07.

Synthesis of 2,6-Bis(Trimethyltin)-4,8-bis(Undec-10-Enyloxy)-Benzo[1,2-b:4,5-b′]di-Thiophene (**3**): To a 100 mL three-necked flask, compound **2** (0.30 g, 0.57 mmol) and 20 mL of anhydrous tetrahydrofuran (THF) were added under argon atmosphere. The resulting solution was cooled to −78 °C and stirred, and then 2.5 M *n*-butyllithium solution in *n*-hexane (0.54 mL, 1.36 mmol) was added dropwise to the solution. After addition the reaction mixture was kept at −78 °C for 2 h with stirring, and then trimethyltin chloride (293.2 mg, 1.47 mmol) was added in one portion. The resulting mixture was allowed to warm to room temperature and stirred overnight. After workup, the reaction mixture was poured into saturated potassium fluoride aqueous solution and stirred for 30 min, then extracted with ethyl acetate for three times. The combined organic phase was washed with brine, dried over anhydrous Na_2SO_4, filtered, and concentrated. Recrystallization of the residue from acetonitrile yield compound **3** as a yellow solid (300 mg, 62%). ^{1}H NMR(400 MHz, $CDCl_3$), δ (ppm): 7.51 (s, 1H), 5.91–5.72 (m, 1H),

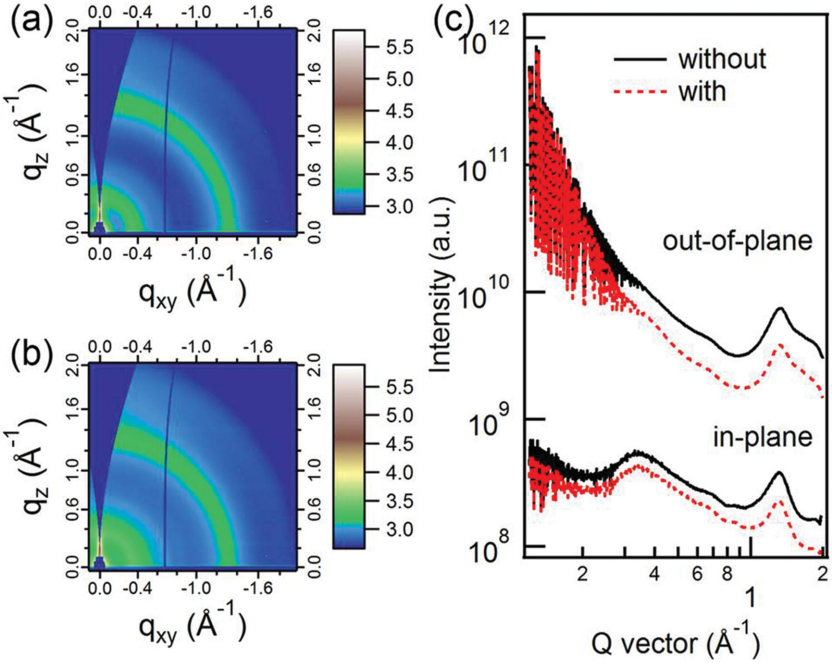

Figure 6. 2D GIWAXS patterns of PTB7:$PC_{71}BM$ active layer a) without and b) with **PTB7-TV** as MIL. c) Line-cut of GIWAXS patterns in the in-plane and out-of-plane direction.

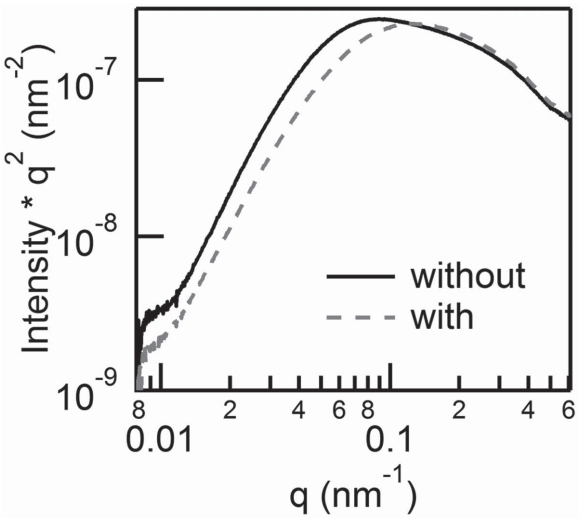

Figure 7. R-SoXS profiles in log scale for PTB7:$PC_{71}BM$ active layer with and without **PTB7-TV** as MIL.

5.06–4.87 (m, 2H), 4.29 (*t*, *J* = 6.6 Hz, 2H), 2.12–1.96 (m, 2H), 1.94–1.80 (m, 2H), 1.63–1.55 (m, 2H), 1.44–1.26 (m, 10H), 0.44 (s, 9H). ^{13}C NMR (101 MHz, $CDCl_3$) δ (ppm): 143.12, 140.49, 139.23, 134.03, 132.99, 128.02, 114.12, 73.59, 33.82, 30.55, 29.63, 29.48, 29.17, 28.96, 26.12, –8.32.

Synthesis of **PTB7-TV**: A mixture of di-tin monomer **3** (240.1 mg, 0.282 mmol.), di-bromo monomer **4** (133.0 mg, 0.282 mmol), $Pd_2(dba)_3$ (5.2 mg, 0.006 mmol), P(*o*-tolyl)$_3$ (6.9 mg, 0.023 mmol), degassed toluene (9 mL), and degassed N,N-dimethylformamide (DMF) (1.5 mL) were vigorously stirred at 120 °C under argon atmosphere. After 36 h, bromobenzene (0.1 mL) was added to the reaction mixture and stirred for 4 h. After cooled down, the resulting mixture was poured into methanol (100 mL) and the precipitate was collected by filtration. The crude polymer was washed in a Soxhlet apparatus with acetone, *n*-hexane, and THF in sequential order. The THF fraction was concentrated and poured into methanol. The polymer fiber was recovered by filtration and dried in vacuum overnight. Yield: 0.18 g, 80%. ^1H NMR (400 MHz, $CDCl_3$), δ (ppm): 7.65–7.56 (br, 2H), 5.73–4.85 (m, 6H), 4.50–4.10 (m, 6H), 1.97–0.96 (m, 47H). Anal. Calcd. for $C_{47}H_{61}FO_4S_4$: C, 67.42; H, 7.34; S, 15.32. Found: C, 67.35; H, 7.41; S, 15.01. GPC (THF, polystyrene standard), M_n = 15200, PDI = 3.5.

Supporting Information

Supporting Information is available from the Wiley Online Library or from the author.

Acknowledgements

This work was financially supported by the 973 Project (Grant Nos. 2014CB643504 and 2015CB655001), the Nature Science Foundation of China (Grant No. 51373165), the Strategic Priority Research Program of Chinese Academy of Sciences (Grant No. XDB12010200), and the "Thousand Talents Program" of China. X-ray data was acquired at beamlines 7.3.3[23] and 11.0.1.2[20d] at the Advanced Light Source, which was supported by the Director, Office of Science, Office of Basic Energy Sciences, of the U.S. Department of Energy under Contract No. DE-AC02-05CH11231.

Received: September 10, 2015
Revised: October 3, 2015
Published online:

[1] a) C. J. Brabec, M. Heeney, I. McCulloch, J. Nelson, *Chem. Soc. Rev.* **2011**, *40*, 1185; b) J. Peet, A. J. Heeger, G. C. Bazan, *Acc. Chem. Res.* **2009**, *42*, 1700; c) J. W. Chen, Y. Cao, *Acc. Chem. Res.* **2009**, *42*, 1709; d) C. Muller, T. A. M. Ferenczi, M. Campoy-Quiles, J. M. Frost, D. D. C. Bradley, P. Smith, N. Stingelin-Stutzmann, J. Nelson, *Adv. Mater.* **2008**, *20*, 3510; e) X. Yang, J. Loos, *Macromolecules* **2007**, *40*, 1353; f) S. E. Shaheen, C. J. Brabec, N. S. Sariciftci, F. Padinger, T. Fromherz, J. C. Hummelen, *Appl. Phys. Lett.* **2001**, *78*, 841; g) J. J. M. Halls, A. C. Arias, J. D. MacKenzie, W. S. Wu, M. Inbasekaran, E. P. Woo, R. H. Friend, *Adv. Mater.* **2000**, *12*, 498; h) S. Q. Zhang, L. Ye, W. C. Zhao, B. Yang, Q. Wang, J. H. Hou, *Sci. China-Chem.* **2015**, *58*, 248.

[2] a) J. A. Bartelt, Z. M. Beiley, E. T. Hoke, W. R. Mateker, J. D. Douglas, B. A. Collins, J. R. Tumbleston, K. R. Graham, A. Amassian, H. Ade, J. M. J. Frechet, M. F. Toney, M. D. McGehee, *Adv. Energy Mater.* **2013**, *3*, 364; b) F. Liu, Y. Gu, J. W. Jung, W. H. Jo, T. P. Russell, *J. Polym. Sci. Pol. Phys.* **2012**, *50*, 1018; c) L. M. Chen, Z. R. Hong, G. Li, Y. Yang, *Adv. Mater.* **2009**, *21*, 1434; d) B. C. Thompson, J. M. J. Frechet, *Angew. Chem. Int. Edit.* **2008**, *47*, 58; e) X. N. Yang, J. Loos, S. C. Veenstra, W. J. H. Verhees, M. M. Wienk, J. M. Kroon, M. A. J. Michels, R. A. J. Janssen, *Nano Lett.* **2005**, *5*, 579.

[3] a) X. Guo, M. J. Zhang, W. Ma, L. Ye, S. Q. Zhang, S. J. Liu, H. Ade, F. Huang, J. H. Hou, *Adv. Mater.* **2014**, *26*, 4043; b) S. A. Mauger, L. L. Chang, S. Friedrich, C. W. Rochester, D. M. Huang, P. Wang, A. J. Moule, *Adv. Funct. Mater.* **2013**, *23*, 1935; c) C. M. Liu, M. S. Su, J. M. Jiang, Y. W. Su, C. J. Su, C. Y. Chen, C. S. Tsao, K. H. Wei, *ACS Appl. Mater. Inter.* **2013**, *5*, 5413; d) D. Yuan, Z. J. Chen, L. X. Xiao, L. P. Mu, B. Qu, Q. H. Gong, *Spectrosc. Spect. Anal.* **2011**, *31*, 3175; e) Y. Vaynzof, D. Kabra, L. H. Zhao, L. L. Chua, U. Steiner, R. H. Friend, *ACS Nano* **2011**, *5*, 329; f) Z. Xu, L. M. Chen, G. W. Yang, C. H. Huang, J. H. Hou, Y. Wu, G. Li, C. S. Hsu, Y. Yang, *Adv. Funct. Mater.* **2009**, *19*, 1227; g) C. R. McNeill, J. J. M. Halls, R. Wilson, G. L. Whiting, S. Berkebile, M. G. Ramsey, R. H. Friend, N. C. Greenham, *Adv. Funct. Mater.* **2008**, *18*, 2309.

[4] a) N. E. Widjonarko, P. Schulz, P. A. Parilla, C. L. Perkins, P. F. Ndione, A. K. Sigdel, D. C. Olson, D. S. Ginley, A. Kahn, M. F. Toney, J. J. Berry, *Adv. Energy Mater.* **2014**, *4*, 1301879; b) M. D. Clark, M. L. Jespersen, R. J. Patel, B. J. Leever, *ACS Appl. Mater. Inter.* **2013**, *5*, 4799; c) Y. Sun, S. C. Chien, H. L. Yip, K. S. Chen, Y. Zhang, J. A. Davies, F. C. Chen, B. P. Lin, A. K. Y. Jen, *J. Mater. Chem.* **2012**, *22*, 5587; d) P. G. Karagiannidis, N. Kalfagiannis, D. Georgiou, A. Laskarakis, N. A. Hastas, C. Pitsalidis, S. Logothetidis, *J. Mater. Chem.* **2012**, *22*, 14624; e) A. F. Tillack, K. M. Noone, B. A. MacLeod, D. Nordlund, K. P. Nagle, J. A. Bradley, S. K. Hau, H. L. Yip, A. K. Y. Jen, G. T. Seidler, D. S. Ginger, *ACS Appl. Mater. Inter.* **2011**, *3*, 726.

[5] C. G. Wu, C. H. Chiang, H. C. Han, *J. Mater. Chem. A* **2014**, *2*, 5295.

[6] G. W. Kim, G. Y. Lee, B. J. Moon, H. I. Kim, T. Park, *Org. Electron.* **2014**, *15*, 3268.

[7] Z. G. Xiao, Y. B. Yuan, B. Yang, J. VanDerslice, J. H. Chen, O. Dyck, G. Duscher, J. S. Huang, *Adv. Mater.* **2014**, *26*, 3068.

[8] a) Z. H. Chen, P. Cai, J. W. Chen, X. C. Liu, L. J. Zhang, L. F. Lan, J. B. Peng, Y. G. Ma, Y. Cao, *Adv. Mater.* **2014**, *26*, 2586; b) Y. F. Deng, J. Liu, J. T. Wang, L. H. Liu, W. L. Li, H. K. Tian, X. J. Zhang, Z. Y. Xie, Y. H. Geng, F. S. Wang, *Adv. Mater.* **2014**, *26*, 471; c) Y. H. Liu, J. B. Zhao, Z. K. Li, C. Mu, W. Ma, H. W. Hu, K. Jiang, H. R. Lin, H. Ade, H. Yan, *Nat. Commun.* **2014**, *5*, 5293.

[9] a) S. C. Chien, F. C. Chen, M. K. Chung, C. S. Hsu, *J. Phys. Chem. C* **2012**, *116*, 1354; b) I. P. Murray, S. J. Lou, L. J. Cote, S. Loser, C. J. Kadleck, T. Xu, J. M. Szarko, B. S. Rolczynski, J. E. Johns, J. X. Huang, L. P. Yu, L. X. Chen, T. J. Marks, M. C. Hersam, *J. Phys. Chem. Lett.* **2011**, *2*, 3006; c) X. Bulliard, S. G. Ihn, S. Yun, Y. Kim, D. Choi, J. Y. Choi, M. Kim, M. Sim, J. H. Park, W. Choi, K. Cho, *Adv. Funct. Mater.* **2010**, *20*, 4381; d) C. Y. Li, T. C. Wen, T. F. Guo, *J. Mater. Chem.* **2008**, *18*, 4478; e) F. C. Chen, Y. K. Lin, C. J. Ko,

Appl. Phys. Lett. **2008**, *92*, 023307; f) S. Y. Heriot, R. A. L. Jones, *Nat. Mater.* **2005**, *4*, 782.

[10] B. Meng, Y. Y. Fu, Z. Y. Xie, J. Liu, L. X. Wang, *Macromolecules* **2014**, *47*, 6246.

[11] a) D. Wang, F. Liu, N. Yagihashi, M. Nakaya, S. Ferdous, X. B. Liang, A. Muramatsu, K. Nakajima, T. P. Russell, *Nano Lett.* **2014**, *14*, 5727; b) B. A. Collins, Z. Li, J. R. Tumbleston, E. Gann, C. R. McNeill, H. Ade, *Adv. Energy Mater.* **2013**, *3*, 65; c) Z. C. He, C. M. Zhong, S. J. Su, M. Xu, H. B. Wu, Y. Cao, *Nat. Photonics* **2012**, *6*, 591; d) S. J. Lou, J. M. Szarko, T. Xu, L. P. Yu, T. J. Marks, L. X. Chen, *J. Am. Chem. Soc.* **2011**, *133*, 20661; e) Y. Y. Liang, Z. Xu, J. B. Xia, S. T. Tsai, Y. Wu, G. Li, C. Ray, L. P. Yu, *Adv. Mater.* **2010**, *22*, E135; f) Y. Y. Liang, D. Q. Feng, Y. Wu, S. T. Tsai, G. Li, C. Ray, L. P. Yu, *J. Am. Chem. Soc.* **2009**, *131*, 7792.

[12] a) H. L. Yip, A. K. Y. Jen, *Energy Environ. Sci.* **2012**, *5*, 5994; b) S. W. Shelton, T. L. Chen, D. E. Barclay, B. W. Ma, *ACS Appl. Mater. Interfaces* **2012**, *4*, 2534; c) A. W. Hains, C. Ramanan, M. D. Irwin, J. Liu, M. R. Wasielewski, T. J. Marks, *ACS Appl. Mater. Inter.* **2010**, *2*, 175; d) J. C. Bijleveld, R. A. M. Verstrijden, M. M. Wienk, R. A. J. Janssen, *Appl. Phys. Lett.* **2010**, *97*, 073304.

[13] a) L. E. Chen, X. E. Li, Y. W. Chen, *Polym. Chem-Uk* **2013**, *4*, 5637; b) C. H. Yang, J. H. Hou, B. Zhang, S. Q. Zhang, C. He, H. Fang, Y. Q. Ding, J. P. Ye, Y. F. Li, *Macromol. Chem. Phys.* **2005**, *206*, 1311; c) A. E. A. Contoret, S. R. Farrar, P. O. Jackson, M. O'Neill, J. E. Nicholls, S. M. Kelly, G. J. Richards, *Syn. Met.* **2001**, *121*, 1645; d) C. H. Yang, G. F. He, R. Q. Wang, Y. F. Li, *J. Appl. Polym. Sci.* **1999**, *73*, 2535.

[14] L. Y. Lu, T. Y. Zheng, T. Xu, D. L. Zhao, L. P. Yu, *Chem. Mater.* **2015**, *27*, 537.

[15] Q. Y. Xing, R. Q. Xu, Z. Zhou, W. W. Pei, *Basic Organic Chemistry*, Vol. *1*, 2nd ed., Higher Education Press, China **1993**, Ch. 8.

[16] D. K. Owens, R. C. Wendt, *J. Appl. Polym. Sci.* **1969**, *13*, 1741.

[17] a) C. E. Tsai, M. H. Liao, Y. L. Chen, S. W. Cheng, Y. Y. Lai, Y. J. Cheng, C. S. Hsu, *J. Mater. Chem. C* **2015**, *3*, 6158; b) K. Tada, *Sol. Energy Mater. Sol. Cells* **2015**, *132*, 15; c) M. Qian, R. Zhang, J. Y. Hao, W. J. Zhang, Q. Zhang, J. P. Wang, Y. T. Tao, S. F. Chen, J. F. Fang, W. Huang, *Adv. Mater.* **2015**, *27*, 3546; d) S. Guo, B. Y. Cao, W. J. Wang, J. F. Moulin, P. Muller-Buschbaum, *ACS Appl. Mater. Interfaces* **2015**, *7*, 4641; e) H. Choi, H. B. Kim, S. J. Ko, J. Y. Kim, A. J. Heeger, *Adv. Mater.* **2015**, *27*, 892; f) S. Bai, S. S. He, Y. Z. Jin, Z. W. Wu, Z. H. Xia, B. Q. Sun, X. Wang, Z. Z. Ye, F. Gao, S. Y. Shao, F. L. Zhang, *RSC Adv.* **2015**, *5*, 8216; g) C. Gu, Y. C. Chen, Z. B. Zhang, S. F. Xue, S. H. Sun, C. M. Zhong, H. H. Zhang, Y. Lv, F. H. Li, F. Huang, Y. G. Ma, *Adv. Energy Mater.* **2014**, *4*, 1301771; h) I. P. Murray, S. J. Lou, L. J. Cote, S. Loser, C. J. Kadleck, T. Xu, J. M. Szarko, B. S. Rolczynski, J. E. Johns, J. X. Huang, L. P. Yu, L. X. Chen, T. J. Marks, M. C. Hersam, *J. Phys. Chem. Lett.* **2011**, *2*, 3006.

[18] a) L. P. Zhang, X. Xing, L. L. Zheng, Z. J. Chen, L. X. Xiao, B. Qu, Q. H. Gong, *Sci. Rep-Uk* **2014**, *4*, 5071; b) F. Monestier, J. J. Simon, P. Torchio, L. Escoubas, F. Florya, S. Bailly, R. de Bettignies, S. Guillerez, C. Defranoux, *Sol. Energy Mater. Sol. Cells* **2007**, *91*, 405; c) L. J. A. Koster, E. C. P. Smits, V. D. Mihailetchi, P. W. M. Blom, *Phys. Rev. B* **2005**, *72*, 085205.

[19] a) W. T. Li, L. Q. Yang, J. R. Tumbleston, L. Yan, H. Ade, W. You, *Adv. Mater.* **2014**, *26*, 4456; b) A. A. Y. Guilbert, J. M. Frost, T. Agostinelli, E. Pires, S. Lilliu, J. E. Macdonald, J. Nelson, *Chem. Mater.* **2014**, *26*, 1226.

[20] a) S. Mukherjee, C. M. Proctor, J. R. Tumbleston, G. C. Bazan, T. Q. Nguyen, H. Ade, *Adv. Mater.* **2015**, *27*, 1105; b) W. Ma, J. R. Tumbleston, L. Ye, C. Wang, J. H. Hou, H. Ade, *Adv. Mater.* **2014**, *26*, 4234; c) W. Ma, J. R. Tumbleston, M. Wang, E. Gann, F. Huang, H. Ade, *Adv. Energy Mater.* **2013**, *3*, 864; d) E. Gann, A. T. Young, B. A. Collins, H. Yan, J. Nasiatka, H. A. Padmore, H. Ade, A. Hexemer, C. Wang, *Rev. Sci. Instrum.* **2012**, *83*, 045110.

[21] B. A. Collins, Z. Li, J. R. Tumbleston, E. Gann, C. R. McNeill, H. Ade, *Adv. Energy Mater.* **2013**, *3*, 65.

[22] S. Albrecht, S. Janietz, W. Schindler, J. Frisch, J. Kurpiers, J. Kniepert, S. Inal, P. Pingel, K. Fostiropoulos, N. Koch, D. Neher, *J. Am. Chem. Soc.* **2012**, *134*, 14932.

[23] A. Hexemer, W. Bras, J. Glossinger, E. Schaible, E. Gann, R. Kirian, A. MacDowell, M. Church, B. Rude, H. Padmore, *J. Phys. Conf. Ser.* **2010**, *247*, 012007.